Vista aérea río Cananarí-Vaupés. Foto: Diana Mora

Trend analysis of precipitation, evapotranspiration and soil moisture in regions under different regimes of forest loss in Amazonia

Elizabeth Arango-Ruda[1,*], Germán Poveda[1]

Abstract

Water vapor (H_2O) exchange between the biosphere and the atmosphere plays a central role in the regional and global and continental climate system. Particularly, tropical forests are essential in the global water cycle and the Amazon rainforest in South America's. This study analyzes the monthly variability of rainfall, evapotranspiration, and soil moisture trends at 38 sub-basins throughout the Amazon rainforest for 2001-2019. The Mann-Kendall test was used to determine the existence and statistical significance of the trends for all sub-basins and the Sen's slope was used to estimate their magnitude. Our results showed that sub-basins located at the "Arc of Deforestation" (south-eastern Amazonia) showed decreasing trends in the hydroclimatic variables, validating the influence of land cover on the climate and hydrology of this region. The mean value of negative trends for hydroclimatic variables was -0.15 mm month^{-1} (precipitation), -0.06 mm month^{-1} (soil moisture) and -0.5 mm month^{-1} (evapotranspiration). Some nearby sub-basin with different forest loss percentages showed contrasting trends in the hydroclimatic variables. Our results confirm the deleterious impacts of deforestation on the hydrologic cycle, which have enormous implications for ecosystem functioning and sustainable management.

Keywords: Remote sensing, Evapotranspiration; Precipitation; Soil Moisture; deforestation; Global Forest Watch

Resumen

El intercambio de vapor de agua (H_2O) entre la biosfera y la atmósfera juega un papel central en el sistema climático regional, global y continental. En particular, los bosques tropicales son esenciales en el ciclo mundial del agua y la selva amazónica lo es en el ciclo de América del Sur. Este estudio analiza la variabilidad mensual de las tendencias de lluvia, evapotranspiración y humedad del suelo en 38 sub-cuencas, a lo largo y ancho de la selva amazónica, entre 2001-2019. Para determinar la existencia y significación estadística de las tendencias para todas las subcuencas, se utilizó la prueba de Mann-Kendall y la pendiente de Sen, para estimar su magnitud. Nuestros resultados mostraron que las subcuencas ubicadas en el "Arco de deforestación" (sureste de la Amazonia), revelaron tendencias decrecientes en las variables hidroclimáticas, validando la influencia de la cobertura vegetal en el clima y la hidrología de esta región. El valor medio de las tendencias negativas para las variables hidroclimáticas fue de -0,15 mm $^{mes-1}$ (precipitación), -0,06 mm $^{mes-1}$ (humedad del suelo) y -0,5 mm $^{mes-1}$ (evapotranspiración). Algunas subcuencas cercanas, con diferentes porcentajes de pérdida de bosques, mostraron tendencias contrastantes en las variables hidroclimáticas. Nuestros resultados confirman los impactos nocivos de la deforestación en el ciclo hidrológico, con enormes implicaciones para el funcionamiento de los ecosistemas y la gestión sostenible.

Palabras clave: Cambio climático, tendencias, pérdida de bosque, Amazonia

---

[1] Departmento de Geociencias y Medio Ambiente, Universidad Nacional de Colombia, Medellín, Colombia
* earangor@unal.edu.co

INTRODUCTION

Forests are globally significant for their capacity of providing benefits such as goods and services (e.g., clean water and healthy soils), livelihood support, ecosystem regulation, and harbor of terrestrial biodiversity (Bonan, 2008). Tropical forests serve as carbon sinks and maintain biodiversity, containing up to 40% of the carbon stored as terrestrial biomass and representing 30% to 50% of the world's forest productivity (Phillips et al., 1998). In the last 40 years, the Brazilian Amazon region has witnessed intense rates of deforestation, in particular in the so-called "Arc of Deforestation" located in the states of Acre, Rondônia, South Amazon, and North of Mato Grosso, mainly to extend the agricultural frontier (Alves et al., 2017). Land use and vegetation cover changes associated with deforestation transform the biotic component of ecosystems and alter their innumerable ecological functions, as well as the biogeophysical processes that are involved in the dynamics of soil-atmosphere interaction, resulting in changes in water and energy balances (Foley et al., 2013)a range of regional climate models have been used to test approaches to Bayesian model averaging (BMA, contributing to and intensifying climate change's impacts. Land cover changes can modify the flux of latent heat to the atmosphere, atmospheric circulation patterns and land surface temperature, among others.

The analysis of trends has been used extensively across regions and hydro-climatic time series to identify sources of variability. The Mann-Kendall and Sen tests have been extensively used to assess the statistical significance and magnitude of the trends, respectively (Adarsh & Shyma, 2017; Almeida et al., 2017; Carmona & Poveda, 2014; Sayemuzzaman & Jha, 2014). Previous works indicate mixed trends in the hydroclimatic variables of the Amazon basin. Almeida et al. (2017) found a positive trend through the Brazilian Legal Amazon for 1973-2013. Marengo (2004) found negative precipitation trends for the Amazon for the period 1928-1198, with primarily positive trends in northern Amazonia and negative trends in southern Amazonia. The study of Posada-Gil and Poveda (2015) found increasing trends in 55 streamflow series (49%), decreasing trends in 45 streamflow series (39%), and 14 streamflow series (15%) without any statistically significant trend. Those authors also found a clear-cut power law relating the magnitudes of the identified trends with drainage area, thus pointing out that they are caused by physically consistent mechanisms, of which deforestation and climate change cannot be disregarded, and that the identified trends are not a random statistical artifact. Thorough reviews of the main hydrologic, climatic and biogeochemical impacts of deforestation in Amazonia are included in the studies of Poveda (2020) and Artaxo et al. (2021). The size and location of the Amazon River basin and its outstanding hydroclimatic, ecological and environmental processes make it difficult to identify the causes of specific trends for certain periods. Moreover, the non-linear interaction of land cover (deforestation) and climate change (global warming) simultaneously induces changes in climate trends. For this reason, disentangling the causes of such trends in hydroclimatic time series can be complex. This scenario raises the need to include deforestation data in the analysis of trends.

Most research about the existence of trends have been focused on precipitation and streamflows but have overlooked other fundamental processes making part of the hydrologic cycle such as evapotranspiration and soil moisture. Therefore, in this study, we address the possible existence of trends and signs of hydro-climatic variability in monthly records of precipitation, evapotranspiration, and soil moisture in sub-basins of the Amazon region under different forest loss percentages. This study aimed: (1) To evaluate homogeneity in time series of monthly precipitation, soil moisture, and evapotranspiration; (2) To search for trends in such times series using the Mann-Kendall and Sen tests; and (3) To discuss the obtained trends regarding environmental factors and land cover change. The importance of this work lies in understanding the role of land cover change on the water fluxes in the Amazon basin.

MATERIAL AND METHODS

Study Area

The Amazon River basin lies between 20°S-5°N and 79°-50°W in South America (Figure 1), being the largest river basin in the world with approximately 6.3 million km². The Amazon rainforest covers approximately 5.5 million km² of the basin. The Amazon is characterized for its diversity in landforms: savannas, floodplains, forests, waterfalls, grasslands, plateaus, and regions: Andes Mountains, Northern Fringe area, Southern Fringe area, central region, and coastal area.

The three principal physiographic regions are the sub-andean foreland, the shields, and the continental alluvium. The Intertropical Convergence Zone (ITCZ) influences the region's hydroclimatic seasonality, with a marked wet (November-March) and dry (April-October) seasons, especially in the south. The specific location of the region determines the time of year when the dry or wet season will occur. Intra-annual variability of rainfall is influenced by the South Atlantic convergence zone (SACZ), the South American Low-Level Jet, the Intra-Seasonal Oscillation, the dynamics of diverse aerial rivers, and land surface-atmospheric interactions, among other. The wettest months are March and April. At inter-annual timescales, El Niño-Southern Oscillation (ENSO) is the main modulator of hydroclimatic variability.
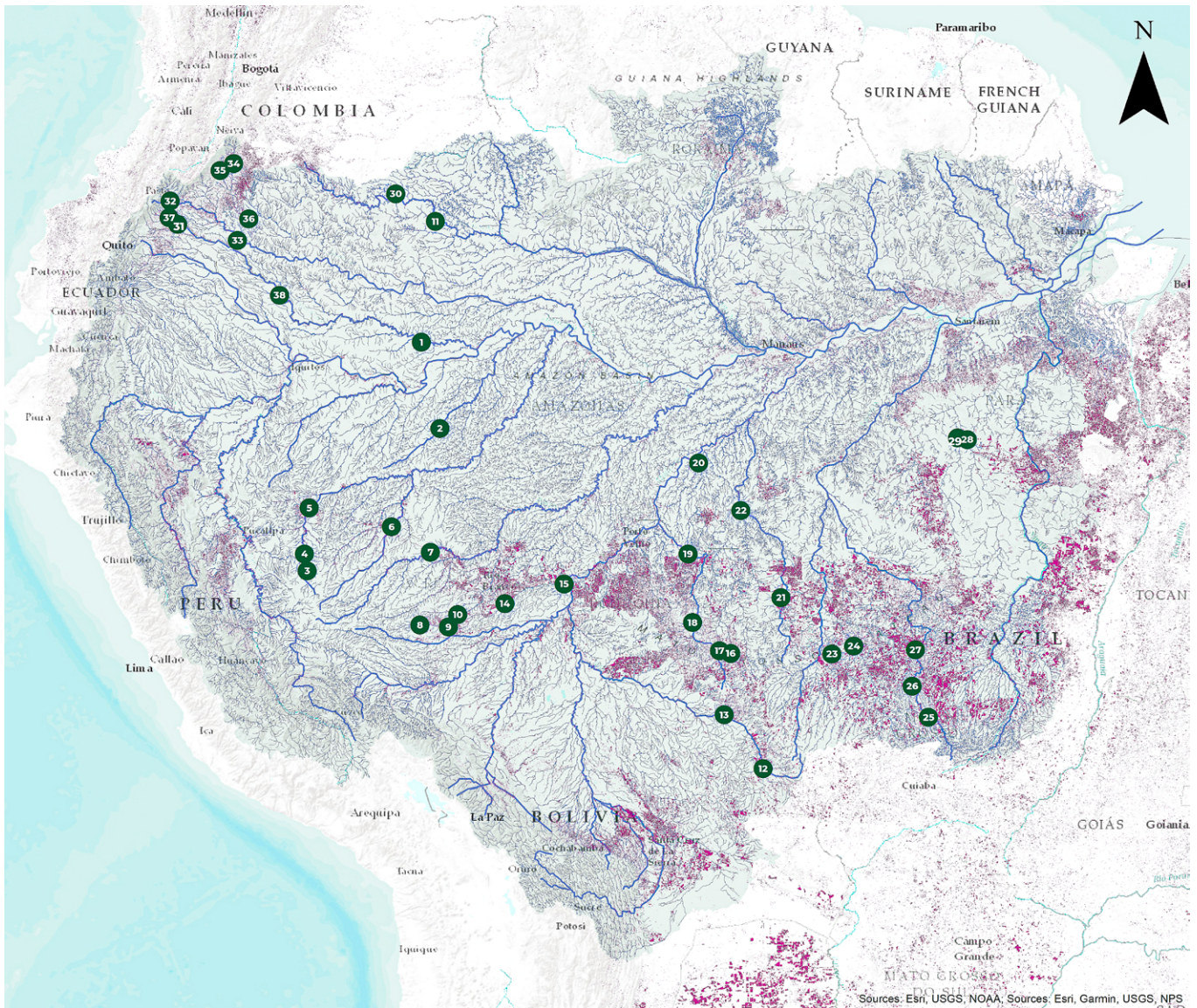
Figure 1. Geographical position and regional distribution of the 38 sub-basins in the Amazon River basin. Color represented intervals of forest loss (%) from Global Forest Watch.

Thirty-eight sub-basins with contrasting percentages of forest loss were included in this work (Figure 1). The basin was chosen regarding the data availability and the degree of comparability. We looked for paired sub-basin with similar geographical locations but different loss rates. Table 1 shows the coordinates of each sub-basin, the area in km², and the river they belong to. Additionally, we show the area (km²) and percentage (%) of tree loss.

Data

In this research, satellite information on hydroclimatic variables was used, including monthly precipitation data from the Tropical Rainfall Measuring Mission (TRMM) and monthly time series of precipitation and soil moisture from the TerraClimate database. For a precise delineation of the different sub-basins within the Amazon river basin, we used the SO HYBAM and HydroSHEDS projects. Some flow stations did not have afferent basins previously generated in these models; in each case, the digital elevation model of WorldClim and SO HYBAM was used to generate the afferent area. By aggregation, we obtained the time series, multiplying each pixel's value by its corresponding area within the basin and averaging each value between the total pixels added (weighted average). The data analysis was carried out in the statistical software R (version 3.4.4) (R Core Team) and the ArcGIS 10.6 software.

Trend analysis of precipitation, evapotranspiration and soil moisture in regions under different regimes of forest loss in Amazonia

11

Table 1. Sub-basin coordinates, area (km²), forest loss (km²) and loss percentage (%) for the period 2001–2016. Loss Information was extracted from the Global Forest Watch raster.

DBN	Station	Area (km²)	Loss (km²)	Loss (%)	River	Latitude (°)	Longitude (°)	Altitude (m)
1	11450000	108535.01	1369.23	1.26	Ica	-2.94	-69.52	76
2	12100000	11065.22	13.02	0.12	Jutaí	-5.38	-69	94
3	12360000	7297.65	31.15	0.43	Juruá	-9.41	-72.72	244
4	12370000	15355.43	208.04	1.35	Juruá	-8.93	-72.79	232
5	12500000	36481.54	1032.19	2.83	Juruá	-7.63	-72.66	175
6	12650000	17277.29	331.87	1.92	Embira	-8.16	-70.36	152
7	13180000	33640.13	248.48	0.74	Purús	-8.88	-69.27	168
8	13450000	3577.28	73.76	2.06	Acre	-10.94	-69.57	232
9	13470000	6947.48	588.56	8.47	Acre	-11	-68.76	192
10	13550000	12574.79	1382.93	11	Acre	-10.65	-68.51	171
11	14260000	41780.82	1020.28	2.44	Uaupés	0.48	-69.13	86
12	15120001	24391.01	2247.17	9.21	Guaporé	-15.01	-59.96	268
13	15130000	56986.16	5501.84	9.65	Guaporé	-13.49	-61.05	193
14	15324000	8842.06	1029.1	11.64	Abuná	-10.34	-67.18	128
15	15326000	31337.73	2633.32	8.4	Abuná	-9.78	-65.53	105
16	15552600	4473.66	870.53	19.46	Comemoraao	-11.75	-60.87	198
17	15552700	17373.57	2884.87	16.6	Apedia ou	-11.68	-61.19	180
18	15560000	30441.63	4364.14	14.34	Ji-Paraná	-10.87	-61.94	133
19	15580000	62400.01	9305.95	14.91	Ji-Paraná	-8.93	-62.06	75
20	15670000	27694.67	887.78	3.21	Marmelos	-6.36	-61.77	46
21	15750000	14242.48	1612.45	11.32	Aripuana	-10.17	-59.46	222
22	15800000	72840.81	7572.21	10.4	Aripuana	-7.71	-60.59	42
23	17095000	27880.12	4094.8	14.69	Do sangue	-11.76	-58.04	269
24	17120000	38147.69	5746.94	15.06	Arinos	-11.54	-57.42	276
25	17200000	12693.6	798.2	6.29	Teles Pires	-13.56	-55.33	434
26	17210000	15918.01	1256.6	7.89	Teles Pires	-12.67	-55.79	386
27	17280000	41507.7	5163.79	12.44	Teles Pires	-11.65	-55.7	373
28	18600000	76457.47	3073.37	4.02	Iriri	-5.7	-54.25	188
29	18650000	43732.76	5138.44	11.75	Curuá	-5.65	-54.52	196
30	42077020	22125.03	837.92	3.79	Vaupés	1.26	-70.24	168
31	44017100	11091.76	720.49	6.5	Putumayo	0.4	-76.34	200
32	44017110	4416.93	32.94	0.75	Caquetá	1.05	-76.55	460
33	44117010	33572.24	2322.54	6.92	Caquetá	-0.06	-74.67	153
34	46017010	3204.04	145.48	4.54	Caguán	2.11	-74.77	670
35	46037060	2477.24	47.53	1.92	Guayas	1.92	-75.15	450
36	46077010	17245.57	2024.41	11.74	Caguán	0.52	-74.28	200
37	47017160	3505.06	173.53	4.95	Putumayo	0.58	-76.58	250
38	47047040	36161.11	1289.79	3.57	Putumayo	-1.61	-73.49	125

DBN – database number

TerraClimate

TerraClimate is a high-resolution global dataset developed by the Climatology Lab, which gathers climatic and hydrological variables of the Earth's surface for the 1958-2015 period at monthly timescales, and spatial resolution of approximately 4 km. TerraClimate uses the climate-enhanced interpolation (CAI) method, combining high spatial resolution climatological standards from the WorldClim dataset with coarser spatial resolution, adopting the period and temporal resolution of the Climate Research Unit (CRU) time-series data version 4.0 (CRU Ts4.0) and the 55-year-old Japanese reanalysis (JRA55). Conceptually, the procedure applies interpolated time variable anomalies from CRU Ts4.0 / JRA55 to high spatial resolution

climatology covering a longer time record. TerraClimate provides information on variables derived from a one-dimensional model of the soil hydrological balance, such as reference evapotranspiration (ASCE Penman-Monteith), runoff (Runoff), Evapotranspiration (Actual Evapotranspiration), climate water deficit (Climate Water Deficit), Soil Moisture, Snow Water Equivalent, Palmer Drought Severity Index and Vapor pressure deficit. The spatial-temporal validation of TerraClimate was carried out using annual information obtained from stations for the variables temperature, precipitation, and reference evapotranspiration, as well as annual runoff measured from flowmeters (Abatzoglou et al., 2018)

TRMM

TRMM was developed by NASA and the Japanese Aerospace Exploration Agency (JAXA) to monitor and study the spatial and temporal dynamics of rainfall in the tropical and subtropical region, between 35° N and 35° S (Braun et al., 2011). From the information obtained by the sensor and through a series of systematized algorithms, estimates of surface precipitation are made with a spatial and temporal resolution of 0.25 ° x 0.25 ° and 3 hours, respectively. TRMM data can be freely available from the NASA website (https://trmm.gsfc.nasa.gov/). The 3B43 product grid data is available in HDF format with a spatial resolution of 0.25° x 0.25° (27 km x 27 km or 729 km^2), covering the globe between latitude 50° N to 50 ° S. Each pixel represents rainfall estimates (millimeters per month) derived from the TRMM sensor and other data sources (Huffman et al., 2007)as well as gauge analyses where feasible, at fine scales (0.25° × 0.25° and 3 hourly.

Global Forest Watch (GFW)

Global Forest Watch (GFW) is an interactive platform for monitoring forests in near real-time. It was developed by the World Resources Institute (WRI), with the collaboration of organizations from academic, public, and private sectors, such as Google, USAID, University of Maryland (UMD), ESRI, among others (GFW, 2018). Hansen et al. (2013) examined global data from Landsat images to characterize the extent, loss, and gain of forest during the year 2000 to 2016. This information is part of the data set available to GFW and is usually known as "Hansen tree cover change data." The data provided by Hansen et al. (2013) are divided into quadrants of 10 x 10 degrees; each quadrant is made up of six files: Tree canopy cover for year 200 (treecover2000), Global Forest cover gain 2000-2012 (gain), Year of gross forest cover loss event (lossyear), Data mask (datamask), Circa year 2000 Landsat 7 cloud-free image composite (last) (GFW, 2018). Each of these files has an 8-bit radiometric resolution and a spatial resolution of 1 arc second per pixel, that is, approximately 30 meters per pixel above the equator Hansen et al., (2013). In this work, the raster layer called lossyear was used to calculate the annual gross forest cover loss event. (Year of gross forest cover loss event) refers to the removal of trees (from natural forests or plantations) during the period 2000-2016.

Method

Change Point Analysis (Homogeneity analysis)

Change Point Analysis (CPA) was applied to hydroclimatic times series of each sub-basin selected in the Amazon rainforest to check for consistency and homogeneity in the monthly time-series of precipitation, evapotranspiration, and soil moisture. We tested changes in mean throughout the Standard Normal Homogeneity Test (SNHT, parametric), which identifies a sudden change in a mean value of time series (Alexandersson, 1986); the Pettit Test (non-parametric), to detect any significant change of a mean value in time series when the exact time is unknown; the Buishand Test (Ahmad & Deni, 2013)homogeneity tests have been applied at 76 meteorological stations in Peninsular Malaysia from 1975 to 2010 and also 7 stations in Sabah and Sarawak. A twostep approach is followed. First, four homogeneity tests, namely standard normal homogeneity test (SNHT and the Buishand U Test (Buishand, 1984). These tests are described below:

Standard Normal Homogeneity Test (SNHT)

This test was developed by Alexandersson (1986) and modified by Alexandersson & Moberg (1997); a value compares the average of the first d year recorded with the last ones ; this value is obtained with the expression

$$T_k = k\bar{z}_1 - (n-k)\bar{z}_2 \ \ when \ k = 1,2,\dots,n \quad (1)$$

where

$$\bar{z}_1 = \frac{1}{k}\frac{\sum_{i=1}^{k}(y_i + \bar{y})}{s} \ y \ \bar{z}_2 = \frac{1}{n-k}\frac{\sum_{i=k+i}^{n}(y_i - \bar{y})}{s}$$

A high value of in year indicates a significant variation: The test statistic is defined as:

$$T_0 = max_{1 \le k \le 0} T(k)$$

Pettitt Test

Pettit's test is non-parametric test based on Wilcoxon's test (Pettitt, 1979), related to the rank order of the values ignores the normality of the series. The statistic that is used is defined as:

$$X_k = 2\sum_{i=1}^{k} r_i - k(n+1) \ when \ k = 1,2,\dots,n \quad (2)$$

If a point of change occurs in the mean of the series in year, the absolute value of reaches its maximum value.

Buishand Test

This test is of Bayesian origin and refers to a simple model that proposes to detect a change in the mean of series for . The test is based on the cumulative deviation from the mean:

$$S_0^* = 0 \ y \ S_k^* = \sum_{i=1}^{k}(y_i - \bar{y}) \ \ para \ k = 1,2,\dots,n \quad (3)$$

where

$$\underline{y} \ is \ the \ sample \ mean \ (y_1, y_2, \dots., y_n)$$

Trend analysis of precipitation, evapotranspiration and soil moisture in regions under different regimes of forest loss in Amazonia

13

The test is defined as:

$$Q = max_{0 \leq k \leq n} \left| \frac{S_k^*}{S} \right|$$

Buishand U Test

In the Buishan U test (Buishand, 1984), the null hypothesis is the same as in the Buishand test. The test statistic is:

$$U = [n(n + 1)]^{-1} \sum_{i=1}^{n} \left(\frac{S_k}{D_x} \right)^2 \qquad (4)$$

with

$$D_x = \sqrt{n^{-1} \sum_{i=1}^{n} (x_i - \bar{x})} \qquad (5)$$

Empirical mode decomposition

To analyze the different modes of temporal variability of time series, we used the Empirical Mode Decomposition (DME), which was proposed as part of the Hilbert-Huang transform (HHT). It consists of separating the modes of oscillation at different frequencies in a time series, smoothing the uneven amplitudes, and if the original series has at least two extremes: local maximums and minimums. The characteristic time scale is defined by the time elapsed between the extremes. Adjustment envelopes defined by maximums and minimums of a series are generated, then the mean of the envelopes is subtracted from the original series. Details on the algorithm and procedure for the application Empirical Mode Decomposition (EMD) can be found in Rao & Hsu (2008).

Mann – Kendall (MK) trend test for non-autocorrelated data

The Mann-Kendall test (Kendal 1945; Mann 1945) allowed us to identify the significance of the trends, and the magnitude of the change was quantified using the Sen slope estimator (Salmi et al., 2002). These two nonparametric methods do not require that the data conform to a specific distribution, are less sensitive to outliers, and are widely used to quantify trends in time series of environmental data (Chandlet and Scott, 2011). Considering the problem of autocorrelation, the use of the modified Mann-Kendall test is proposed for autocorrelated data. This Mann-Kendall trend test is derived from a rank correlation test for two groups of observations considering the correlation between the rank order of the observed values and their order in time.

To apply the Mann-Kendall test, the following procedure is followed:

The MK test statistic S (Mann, 1945, Kendall, 1975) is calculated as

$$S = \sum_{i=1}^{n-1} \sum_{j=i+1}^{n} sign(x_j - x_i) \qquad (6)$$

In Eq. (6), n is the number of data points, and are the data values in time series, i and j are time indexes ($j > i$), respectively and in Eq. (7), sign is the sign function as

$$sign(x_j - x_i) = \begin{cases} +1, if \ (x_j - x_i) > 0 \\ 0, if \ (x_j - x_i) = 0 \\ -1, if \ (x_j - x_i) < 0 \end{cases} \qquad (7)$$

The variance is computed as

$$V(S) = \frac{n(n-1)(2n+5) + \sum_{k=1}^{m} t_k(t_k - 1)(2t_k + 5)}{18} \qquad (8)$$

In eq. (8), n is the number of data points, m is the number of tied groups, and denotes the number of ties of extent k. A tied group is a set of sample data having the same value. In cases where the sample size $n > 10$, the standard normal test statistic is computed using Eq. (9):

$$Z_s = \begin{cases} \frac{S-1}{\sqrt{V(S)}}, & if \ S > 0 \\ 0, & if \ S = 0 \\ \frac{S+1}{\sqrt{V(S)}}, & if \ S < 0 \end{cases} \qquad (9)$$

Comparison of calculated Z and observed Z:

A certain probability associated with Z (Z_{crit}) is calculated with a prescribed significance level ($\alpha = 0.05$, for a 95% confidence level). Therefore, if the Z test statistic is less that the Z_{crit} statistic, then the identified trend is not significant.

Sen's slope

The magnitude of the trend is calculated using the no-parametric Sen test. Sen's statistic is given by the median of the slopes of each pair of points in the data set. The slope is estimated as follows,

$$m = \frac{x_{i+1} - x_i}{(i+1) - i} \qquad (10)$$

Where m is the local slope between the consecutive data and, in the time , and a time , respectively. In this way, the general slope of the series studied results from the median of the entire set of local slopes (Sen, 1968).

Results and discussion

Loss distribution and seasonality of hydroclimatic time series

The 38 sub-basins analyzed in this study were classified into three groups according to their location and land cover characteristics: Southwest Amazon, Southeastern Amazon, and Northern Amazon. The higher level of deforestation was found in sub-basins located at the Arc of Deforestation of Brazil (South and Southeastern Amazonian). Following the classification of MapBiomas (2019), we identified the following land cover use of the study area: Formation (Forest), Non-Forest Natural Formation (Other Non-Forest Formation), Agricultural land and savanna formation for Southeastern Amazon; Forest Formation (Forest), Formation Natural Non-Forest (Other Non-Forest Formation) and Agricultural Use Sub-basins in Southwest Amazon, showing a lower rate of forest loss and up to up 16% of loss; and Forest Formation (Forest) and Agricultural Use in North Amazon (referred to Colombian region) where the loss percentage was up to 11.75%. Figure 2 shows the percentage of loss in the selected sub-basins. Colors closer to red indicate higher rates of loss. Table 1 shows the area of loss and the percentage of loss for each sub-basin.
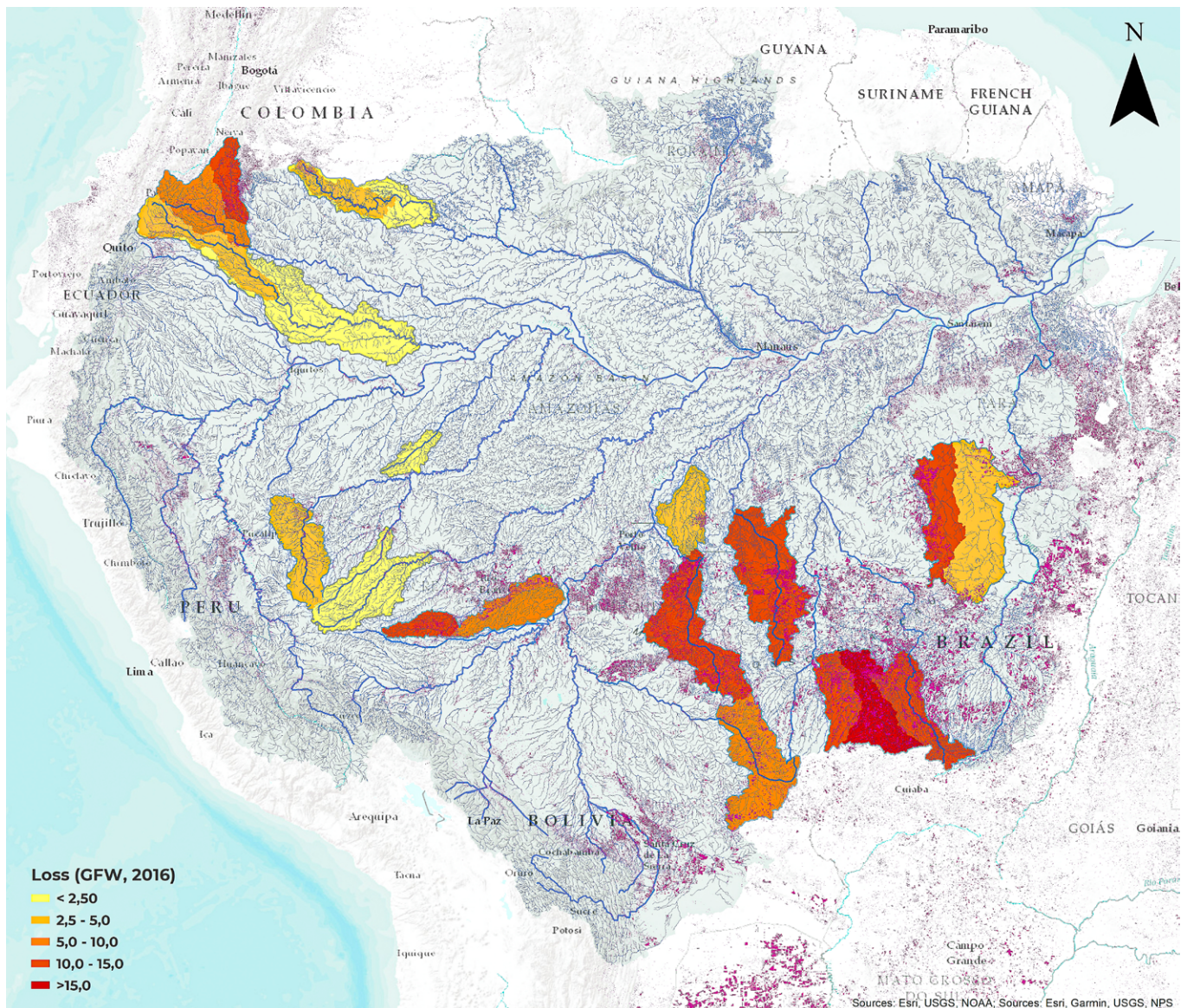

Figure 2. Geographical position and regional distribution of the 38 sub-basin in the Amazon basin. Color represented intervals of forest loss (%) from Global Forest Watch.

Trend analysis of precipitation, evapotranspiration and soil moisture in regions under different regimes of forest loss in Amazonia

Figure 3 shows the Hovmoller diagram of precipitation for the sample of paired basins that showed contrasting trends. Precipitation in the south of the Amazon showed a unimodal annual with two distinctive seasons: dry (June to September) and wet (November to May). Values of monthly precipitation during wet months reached ~ 500 mm. Sub-basins located in north Amazon showed a weak seasonality in the precipitation regime; however, a bimodal annual cycle was identified, where March to May and October to November are the wetter months due to the double pass of the Intertropical Convergence Zone (ITCZ), the main meteorological phenomenon that influences rainfall in the Amazon (Reboita et al., 2010).

Long-term mean precipitation in these sub-basins varied from 1923 to 2190 mm yr^{-1} (Table 2). The seasonality of ET is not clear; however, we identified higher values of ET from September to December (three months, ~ 140 mm) in south Amazon basins, but from January to May in North Amazon sub-basins (~ 100 mm). There was no clear response of evapotranspiration to precipitation in this selected sub-basin. ET increased with the end of the dry season. Lower values of ET are consistent with lower values of P; however, this seasonality is not very contrasting because other factors such as solar radiation, soil moisture in the depth soil can provide the necessary conditions for transpiration of the trees. Total multi-annual precipitation in these sub-basins varied from 922 to 1065.75 mm yr-1 (Table 2).
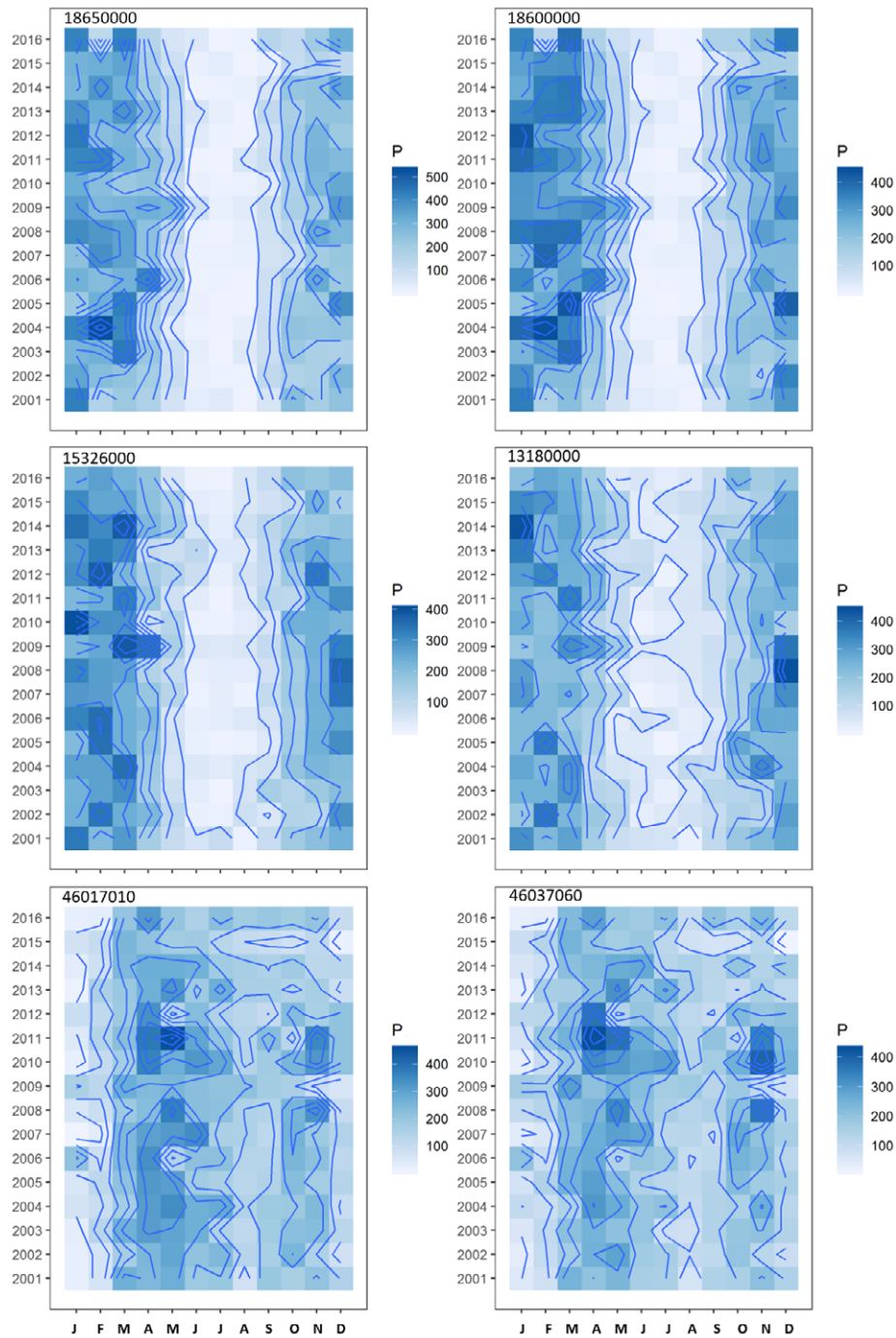
Figure 3. Hovmoller diagram for the precipitation (mm mths^{-1}) from TRMM for the period 2001-2016 in sub-basin with opposite trend in precipitation and contrasting deforestation loss.

Table 2. Multi-year precipitation, evapotranspiration, and soil moisture for sub-basin with contrasting percentage of loss.

DBN	Station	P (Multi-year)	ET (Multi-year)	SM (Multi-year)	Loss (%)	Loss (Total)
29	18650000	2150.69	1065.70	229.12	11.75	5138.44
28	18600000	2113.55	1057.35	246.48	4.02	3073.37
15	15326000	1923.59	993.42	291.8	8.4	2633.32
7	13180000	1987.03	968.21	167.64	0.74	248.48
34	46017010	2190.45	997.60	95.28	4.54	145.48
35	46037060	2069.17	922.63	108.82	1.92	47.53

Trend analysis of precipitation, evapotranspiration and soil moisture in regions under different regimes of forest loss in Amazonia

The Hovmoller diagram of ET for these sub-basins is shown in Figure 4. Soil moisture (SM) showed a strong seasonality in southern Amazon, with a marked unimodal annual cycle. Lower values of SM were recorded from June to November, with a two-month delay with respect to precipitation dry season. Soil moisture showed a strong seasonality in southern Amazon, with a marked unimodal annual cycle; lower values of SM were seen starting June to November, with a delay of two months with respect to precipitation dry season. Soil moisture in northern Amazonia was characterized by low values from January to March and some low values in August-September. Soil moisture typically evidence faint changes in the top layers (Figure 5). A marked seasonal regime is typical in the south and southeastern of the Amazon basin, characterized by longer dry seasons. In the west and northwest of the Amazon, the dry season is typically short or absent (Almeida et al., 2017).
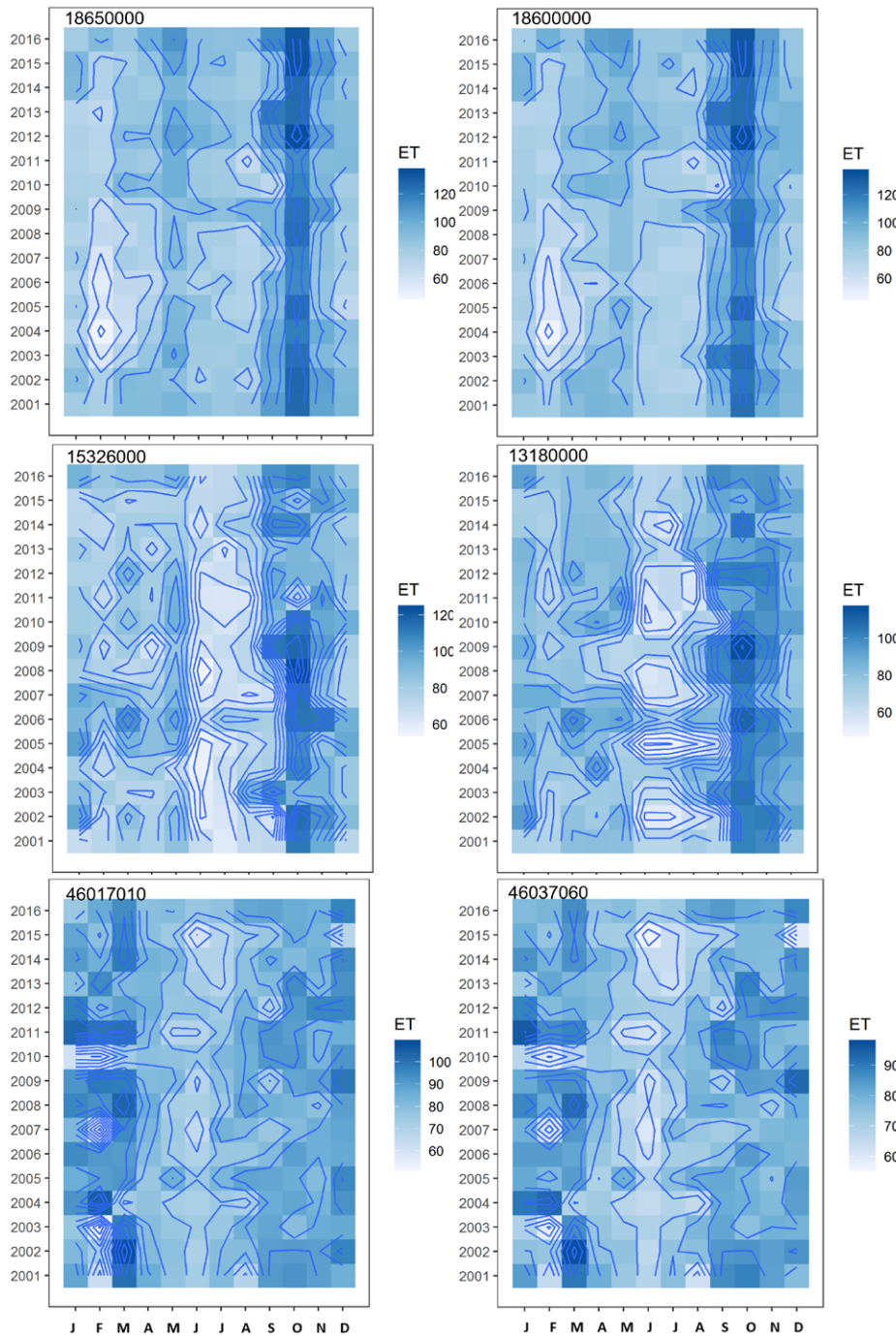

Figure 4. Hovmoller diagram for the evapotranspiration (mm mths^{-1}) from TerraClimate for the period 2001-2016 in sub-basin with opposite trend in precipitation and contrasting deforestation loss.

Testing for homogeneity

The results from the homogeneity tests were classified into three categories:

Class A: Homogeneous or no change point

In these series, in more than one test, the null hypothesis is rejected. In this way, the series is considered homogeneous, and future analyzes can be carried out.

Class B: Doubtful

In these series, the null hypothesis is rejected in two tests. The series in this category are considered to have a sign of inhomogeneity and should be analyzed using other methods.

Class C: Not homogeneous or change point.

Series in which three or more tests indicate that the null hypothesis is rejected. In this case, it is considered that the series does not meet the homogeneity criteria. Table 3 shows
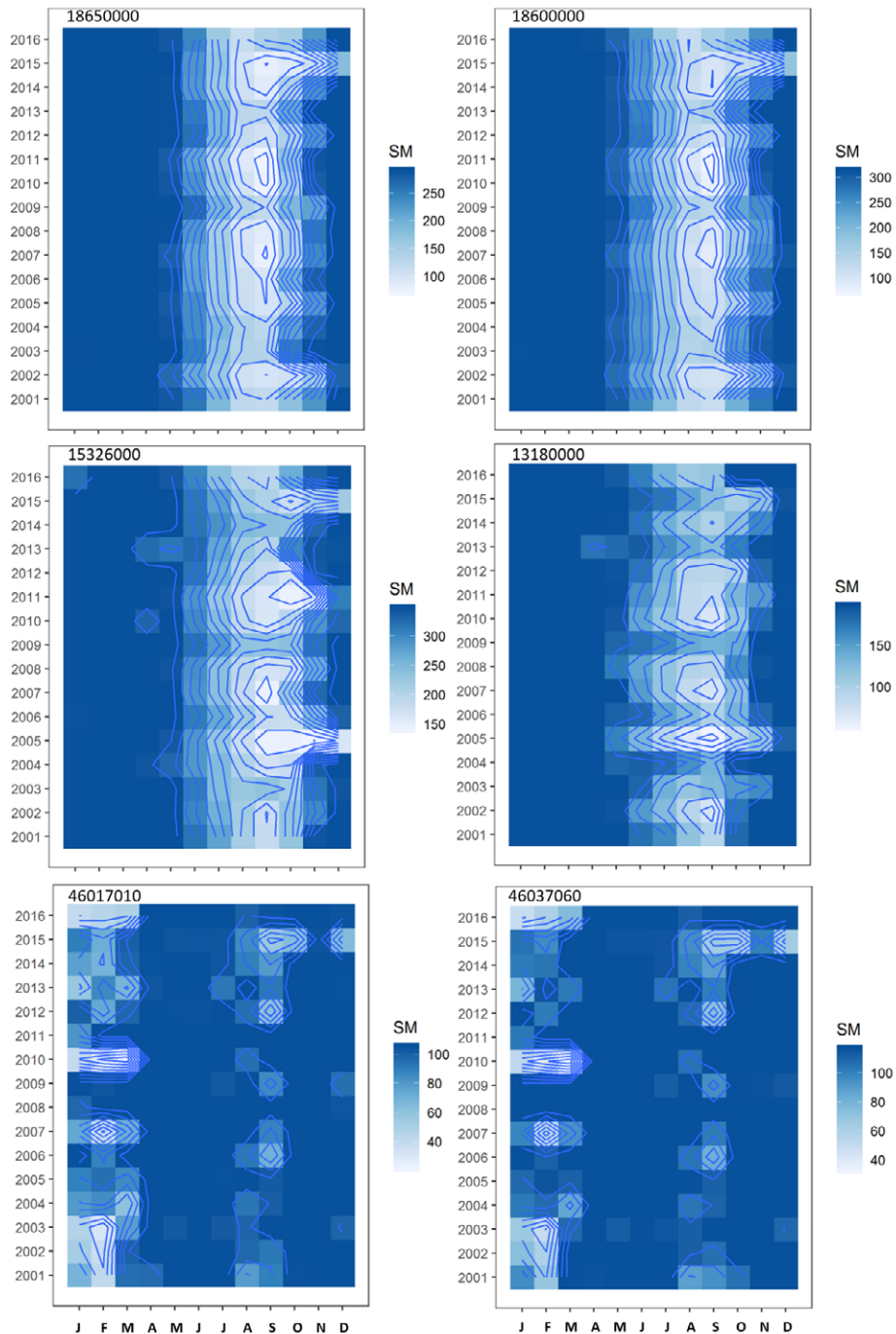

Figure 5. Hovmoller diagram for the soil moisture (mm mths^{-1}) from TerraClimate for the period 2001-2016 in sub-basin with opposite trend in precipitation and contrasting deforestation loss.

Trend analysis of precipitation, evapotranspiration and soil moisture in regions under different regimes of forest loss in Amazonia

results of the the change point detection analysis of precipitation, evapotranspiration, and soil moisture.

The homogeneity analysis showed a non-abrupt change in the time series of monthly precipitation (homogeneity, class A). However, the change point analysis indicated an abrupt change in 2012 in precipitation for basin N32-44017110 (non-homogeneity, class C). The Pettitt test, the SNHT test, and the Buishand U test indicate that 97.4% of the time series are homogeneous. On the other hand, the Buishand test indicates that 86.8% of the series are homogeneous. The tests coincided with the homogeneity result in 89.4% of the analyzed series.

The change point analysis indicates abrupt changes in approximately 30% of ET series (non-homogeneity, class c), while the remaining can be considered homogeneous. Some of the time series presented significant change points in 2004, 2005, 2009 o 2011, with 2005 as the more frequent year of change. As to the particular result of each test, Buishand and SNH tests indicate that 68.4% of the evapotranspiration time series are homogenous. Furthermore, the Pettitt and Buishand U test indicate that 73.7% and 65.8% of the series are homogenous, respectively. The tests coincide in the homogeneity result in most of the series analyzed (80%), but for the stations highlighted with blue color, there is a particular discrepancy among test results. A total of 11 (29%) actual evapotranspiration series are considered non-homogeneous (Class C), while the remaining 27 (71%) are considered homogeneous series (Class A).

As to soil moisture time series, 96% of the series indicate homogeneity for 2001-2016. The Pettitt test, the Buishand test, and the Buishand U test indicate that all soil moisture series are homogeneous (100%), but the SNH test indicates that 84.2% are homogeneous. The soil moisture series were classified as homogenous (Class A), where 8 of the time series have at least one test indicating the presence of non-homogeneity.

Table 3. Results of homogeneity test of climatologic time series (2001 – 2016).

N°	Estación	Precipitation		Soil Moisture		Evapotranspiration	
		Nature of series	Year of shift	Nature of series	Year of shift	Nature of series	Year of shift
1	11450000	A	-	A	-	C	2004
2	12100000	A	-	A	-	C	2009
3	12360000	A	-	A	-	A	-
4	12370000	A	-	A	-	A	-
5	12500000	A	-	A	-	A	-
6	12650000	A	-	A	-	A	-
7	13180000	A	-	A	-	A	-
8	13450000	A	-	A	-	A	-
9	13470000	A	-	A	-	A	-
10	13550000	A	-	A	-	A	-
11	14260000	A	-	A	-	A	-
12	15120001	A	-	A	-	A	-
13	15130000	A	-	A	-	C	2005
14	15324000	A	-	A	-	A	-
15	15326000	A	-	A	-	A	-
16	15552600	A	-	A	-	C	2005
17	15552700	A	-	A	-	C	2005
18	15560000	A	-	A	-	C	2005
19	15580000	A	-	A	-	C	2005
20	15670000	A	-	A	-	C	2009
21	15750000	A	-	A	-	A	-
22	15800000	A	-	A	-	B	-
23	17095000	A	-	A	-	C	2005
24	17120000	A	-	A	-	A	-
25	17200000	A	-	A	-	A	-
26	17210000	A	-	A	-	A	-
27	17280000	A	-	A	-	A	-
28	18600000	A	-	A	-	C	2011
29	18650000	A	-	A	-	C	2011
30	42077020	A	-	A	-	A	-
31	44017100	A	-	A	-	A	-
32	44017110	C	2012	A	-	A	-
33	44117010	A	-	A	-	A	-
34	46017010	A	-	A	-	A	-
35	46037060	A	-	A	-	A	-
36	46077010	A	-	A	-	A	-
37	47017160	A	-	A	-	A	-
38	47047040	A	-	A	-	A	-

Trend analysis

The analysis of trends and the associate statistical and physical significance are essential in hydroclimatic research (NCAR, 2014). Changes and trends commonly found in hydroclimatic time series may be the result of natural phenomena such as volcanic eruptions, forest fires, landslides, climate change on a global, regional, or local scale, solar cycles, among others or human interventions, changes of use soil, change in vegetation cover, change of location of measurement instruments, changes in sampling methodologies, changes in the technology of recording instruments, among others. This section presents the result of the non-parametric Mann-Kendall test and the Sen statistical test to the residual of the series of records of

hydro-climatic variables on which the EMD method was applied, isolating the residue of long term of each series.

Figure 6 shows the time series of precipitation, evapotranspiration, and soil moisture with a corresponding trend line for paired sub-basins with contrasting forest loss percentages and trends. Plots in the left panel show the time series of sub-basins whose precipitation had a decreasing trend, while plots at the right of the panel show the time series of sub-basin with an increasing trend. For the case of these stations, we found a negative trend in precipitation when there is a higher percentage of loss.

Table 4 shows the trend of the hydroclimatic variables for all the time series of the sub-basins considered in this study.
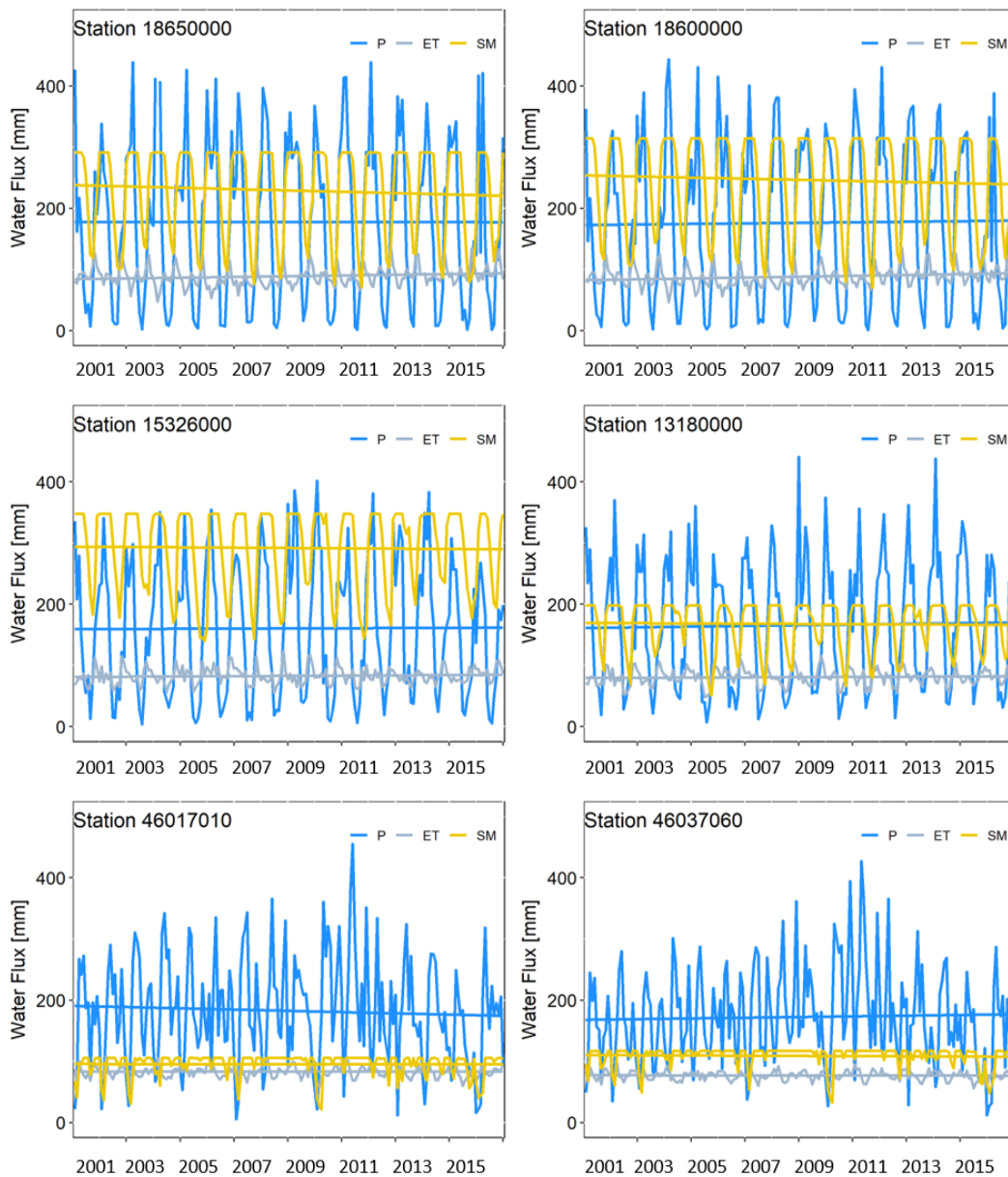

Figure 6. Time series of hydroclimatic variables from 2001 to 2016 for paired basin with contrasting percentages of loss.

Trend analysis of precipitation, evapotranspiration and soil moisture in regions under different regimes of forest loss in Amazonia

Table 4. Results of trend analysis of climatologic time series (2001 – 2016).

N°	Station	Precipitation			Soil Moisture			Evapotranspiration		
		S	Trend (mm mth⁻¹)	Trend (mm mth⁻¹ yr⁻¹)	S	Trend (mm mth⁻¹ yr⁻¹)	Trend (mm mth⁻¹ yr⁻¹)	S	Trend (mm/ mth⁻¹ yr⁻1)	Trend (mm mth⁻¹ yr⁻¹)
1	11450000	1	-0.2479	-2.9753	1	-0.0069	-0.0824	1	0.0291	0.3490
2	12100000	1	0.3784	4.5410	1	-0.0574	-0.6892	1	0.0263	0.3153
3	12360000	1	0.0171	0.2051	1	0.0014	0.0171	1	0.0192	0.2305
4	12370000	1	0.0448	0.5375	1	0.0018	0.0211	1	0.0046	0.0550
5	12500000	1	0.0483	0.5799	1	-0.0162	-0.1939	1	0.0084	0.1009
6	12650000	1	0.0501	0.6010	1	0.0332	0.3985	1	0.0009	0.0103
7	13180000	1	0.0157	0.1885	1	-0.1395	-1.6734	1	-0.0114	-0.1372
8	13450000	1	0.1368	1.6410	1	-0.0519	-0.6226	0	-0.0013	-0.0152
9	13470000	1	0.1596	1.9156	1	-0.0821	-0.9849	1	-0.0037	-0.0443
10	13550000	1	0.1621	1.9448	1	-0.0458	-0.5493	0	-0.0183	-0.2197
11	14260000	1	-0.0180	-0.2162	1	0.0170	0.2041	1	0.0063	0.0761
12	15120001	1	-0.0283	-0.3396	1	0.0602	0.7222	1	-0.0352	-0.4220
13	15130000	0	-0.0033	-0.0390	0	-0.1187	-1.4248	1	-0.0342	-0.4104
14	15324000	1	0.1476	1.7714	1	-0.0380	-0.4560	1	0.0120	0.1435
15	15326000	1	-0.1109	-1.3308	0	-0.0116	-0.1387	1	0.0020	0.0243
16	15552600	1	-0.2007	-2.4078	1	-0.1249	-1.4986	1	-0.0930	-1.1162
17	15552700	1	-0.1461	-1.7536	1	-0.0848	-1.0179	1	-0.0958	-1.1491
18	15560000	1	-0.3594	-4.3129	1	-0.0049	-0.0584	1	-0.0775	-0.9303
19	15580000	1	-0.3973	-4.7675	0	-0.0101	-0.1217	1	-0.0490	-0.5886
20	15670000	1	-0.4871	-5.8453	0	-0.0033	-0.0395	1	0.0326	0.3917
21	15750000	1	-0.1585	-1.9021	0	0.0061	0.0730	0	-0.0217	-0.2609
22	15800000	1	-0.0826	-0.9912	1	-0.1466	-1.7590	0	-0.0104	-0.1248
23	17095000	1	-0.0574	-0.6885	1	-0.1556	-1.8667	1	-0.0757	-0.9089
24	17120000	1	-0.1578	-1.8932	1	-0.1338	-1.6052	1	-0.1018	-1.2216
25	17200000	1	0.0184	0.2209	1	-0.0187	-0.2241	1	-0.1164	-1.3970
26	17210000	1	0.0461	0.5530	1	0.0316	0.3790	1	-0.0748	-0.8981
27	17280000	1	-0.0460	-0.5520	1	-0.0012	-0.0148	1	-0.1069	-1.2830
28	18600000	0	0.0110	0.1321	1	-0.0731	-0.8769	1	0.0679	0.8151
29	18650000	1	-0.1044	-1.2532	1	-0.1558	-1.8695	1	0.0568	0.6817
30	42077020	1	-0.0216	-0.2586	1	-0.0201	-0.2407	1	0.0062	0.0746
31	44017100	0	0.0120	0.1440	1	0.0181	0.2169	1	0.0311	0.3733
32	44017110	1	-0.3154	-3.7853	1	0.0104	0.1246	1	0.0162	0.1947
33	44117010	1	-0.1704	-2.0447	1	-0.0096	-0.1157	1	0.0227	0.2726
34	46017010	1	-0.1167	-1.4004	0	0.0060	0.0724	1	-0.0044	-0.0524
35	46037060	1	0.1527	1.8322	1	-0.0322	-0.3861	1	-0.0109	-0.1311
36	46077010	1	-0.0601	-0.7211	1	-0.0174	-0.2087	1	0.0032	0.0389
37	47017160	1	-0.0526	-0.6314	1	0.0097	0.1158	1	0.0129	0.1543
38	47047040	1	-0.1652	-1.9822	1	-0.0161	-0.1931	1	0.0263	0.3160

There is evidence of a significant trend in 35 of the 38 monthly precipitation series, with an increasing trend in 13 stations (34.0%); decreasing trends in 22 stations (57.89%), and no trend or non-significant trend in 3 stations (7.89%) for 2001-2016 (Figure 7). The trends of precipitation were mainly negative throughout the basin.

Time series of soil moisture showed predominantly significant trends where 23 (60.53%) correspond to decreasing trend and 9 (23.68 %) correspond to increasing trend. Only 6 (15.79%) time series showed no significance. The result indicates a significant decreasing trend in soil moisture in the sub-basing analyzed for 2001-2016 (Figure 8).

When analyzing trends in the monthly evapotranspiration, we found statistically significant increasing trends in 20 (51.3%) time series; statistically significant decreasing trends in 15 (38.5%) time series, and no trend or statistically non-significant trend in 4 (10.3%) time series. There were increasing trends in more than 50% of the monthly actual evapotranspiration series in this period. The increasing trends belong mainly to basins with a loss percentage greater than 10% (Figure 9).

Given the large extension of the Amazon basin, we grouped the sub-basins in three major sub-regions: North, Southwestern, and Southeastern to understand the trends depending on the land cover and magnitude of loss. In Southwestern Amazonia, trends of the hydroclimatic variables were predominately positive: P (90.0%), ET (63%), SM (72.7%). On the contrary, in Southeastern Amazonia, the trend analysis showed decreasing trends for P (81.3%), ET (81.3%), and SM (81.3%). In North Amazonia (Colombian's sub-basins), trends were positive for ET (81.82%), negative for SM (54.5%), and negative for P (81.82%).
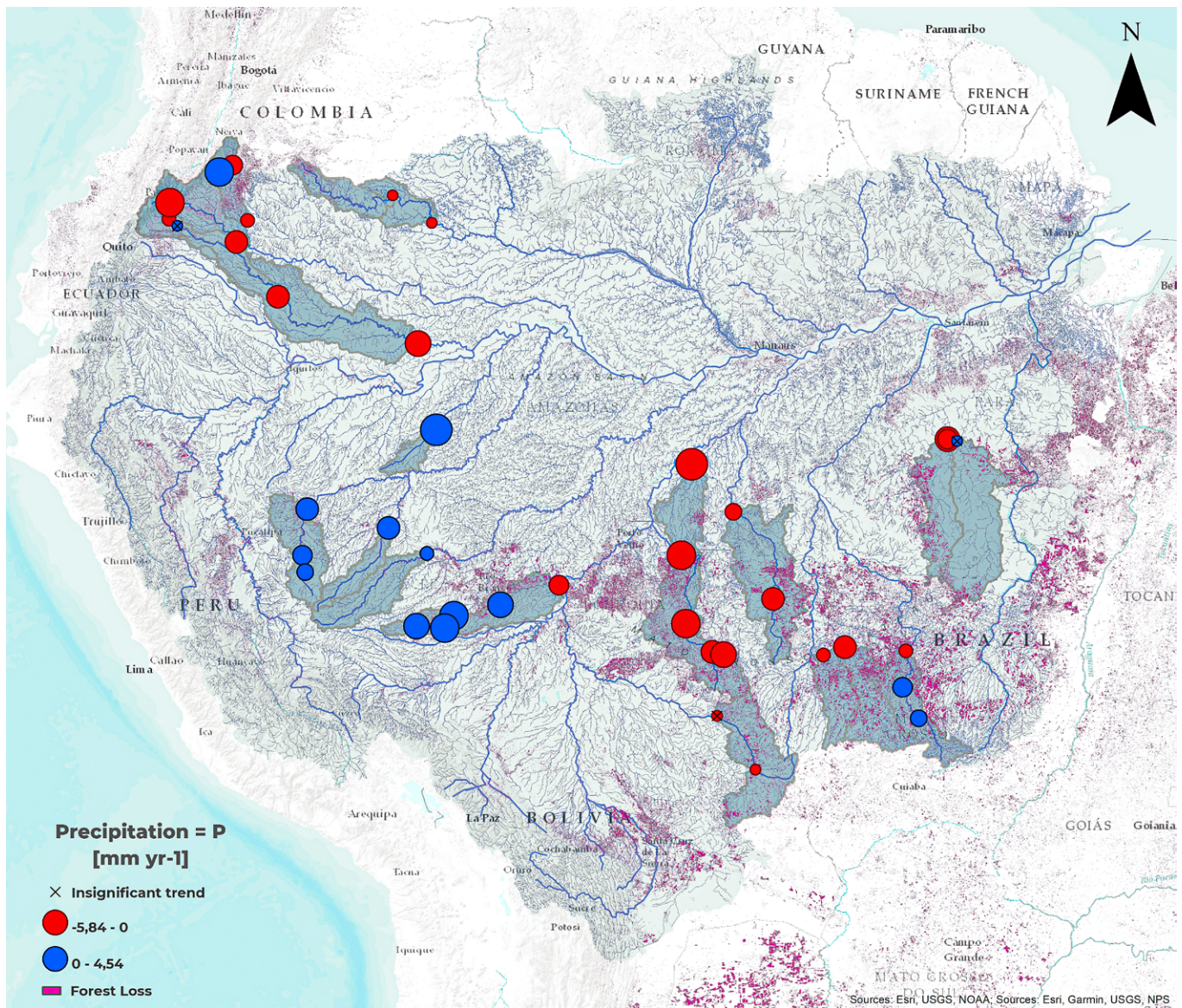
Figure 7. Distribution of trend in precipitation in 38 the selected sub-basins. The color of the circles denote decreasing trends (red) and increasing trends (blue) and the diameter of the circle is correlative with the magnitude of the identified trend. See the convention at the bottom left.

DISCUSSION

Homogeneity analysis

The different tests used present different levels of demand, and therefore differ in some respects. SNHT is sensitive in detecting changes near the beginning and end of the series. The Buishand test and the Pettitt test are close to identifying changes in the middle of the series. Furthermore, the SNHT test and the Buishand test assume that the respective variable be normally distributed, while the Pettitt test does not need this assumption because it is a non-parametric range test (Kang & Yusof, 2018). Therefore, results obtained from the homogeneity test can differ; that is, the same climatic series can be considered

simultaneously as homogeneous by one test and non-homogeneous by another.

In general, our results indicate that the series of the hydro-climatic variables evaluated for 2001-2016 are mainly homogeneous, which would indicate that the existing variations are only due to the variability of the natural dynamics of the variable itself. Consequently, seasonal cycles or conditions are not considered; however, the analysis of seasonal periods, such as the dry season, the wet season, or periods of specific interest, could give greater certainty to the results.

In general, homogeneity in time series reflects the use of similar instruments or the same environment when collected. However, it will always be susceptible to change due to
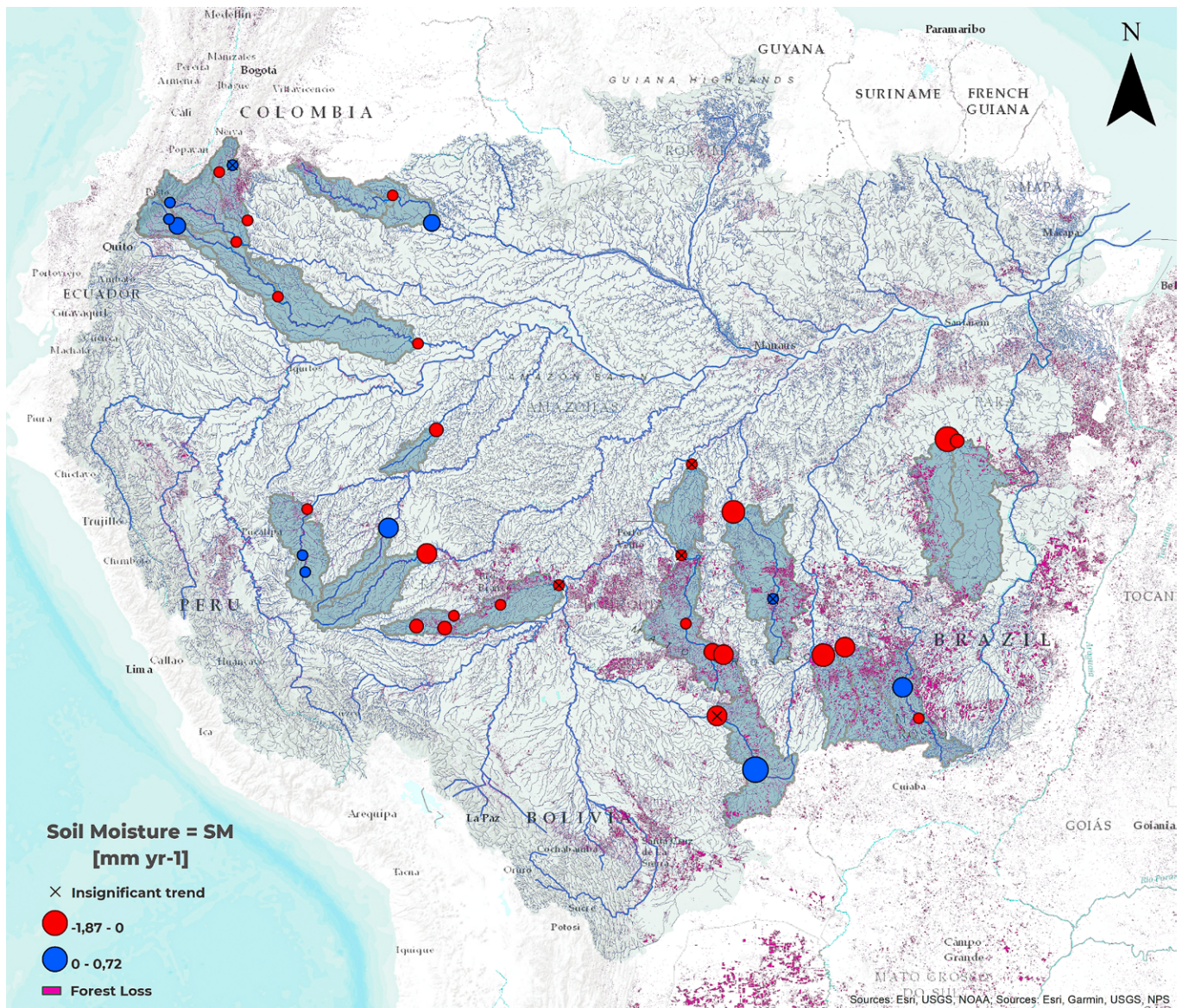
Trend analysis of precipitation, evapotranspiration and soil moisture in regions under different regimes of forest loss in Amazonia

Figure 8. Similar to Fig. 7 for soil moisture trends in the selected sub-basins.

measurement techniques, the observation procedures, the characteristics of the environment, and the location of the stations. Further analysis is required for non-homogenous time series. Abrupt changes in the time series may have a meteorological or climatic origin but may also be due to factors such as spatial location and human or instrumental influence, poor condition, or defects of the observation instruments, change of instrumental type and / or their installation conditions and change in the data purification methods, since it alters them.

For the time series obtained by aggregating satellite information, it is likely that the non-homogeneity is due to issues with the algorithm used to estimate the variable in areas where data is not sufficiently precise in the basin. No homogeneity of time series may be explained by errors of anthropogenic and natural

character, such as land cover and land-use change or climate variability (Kliment et al., 2011).

Trend analysis

We found mixed trends in the sub-basin that were analyzed with no apparent direct individual influence of loss. An increasing trend in Southwestern Amazonia sub-basins (90% of the time series of P and 63% of ET) show evidence of positive values under the scenario where some forests are still present. The fact that some regions with a higher percentage of loss have a positive trend (and the opposite) has to do with the fact some deforested areas that are found side by side with forested areas generate a breeze from the forest to those deforested during
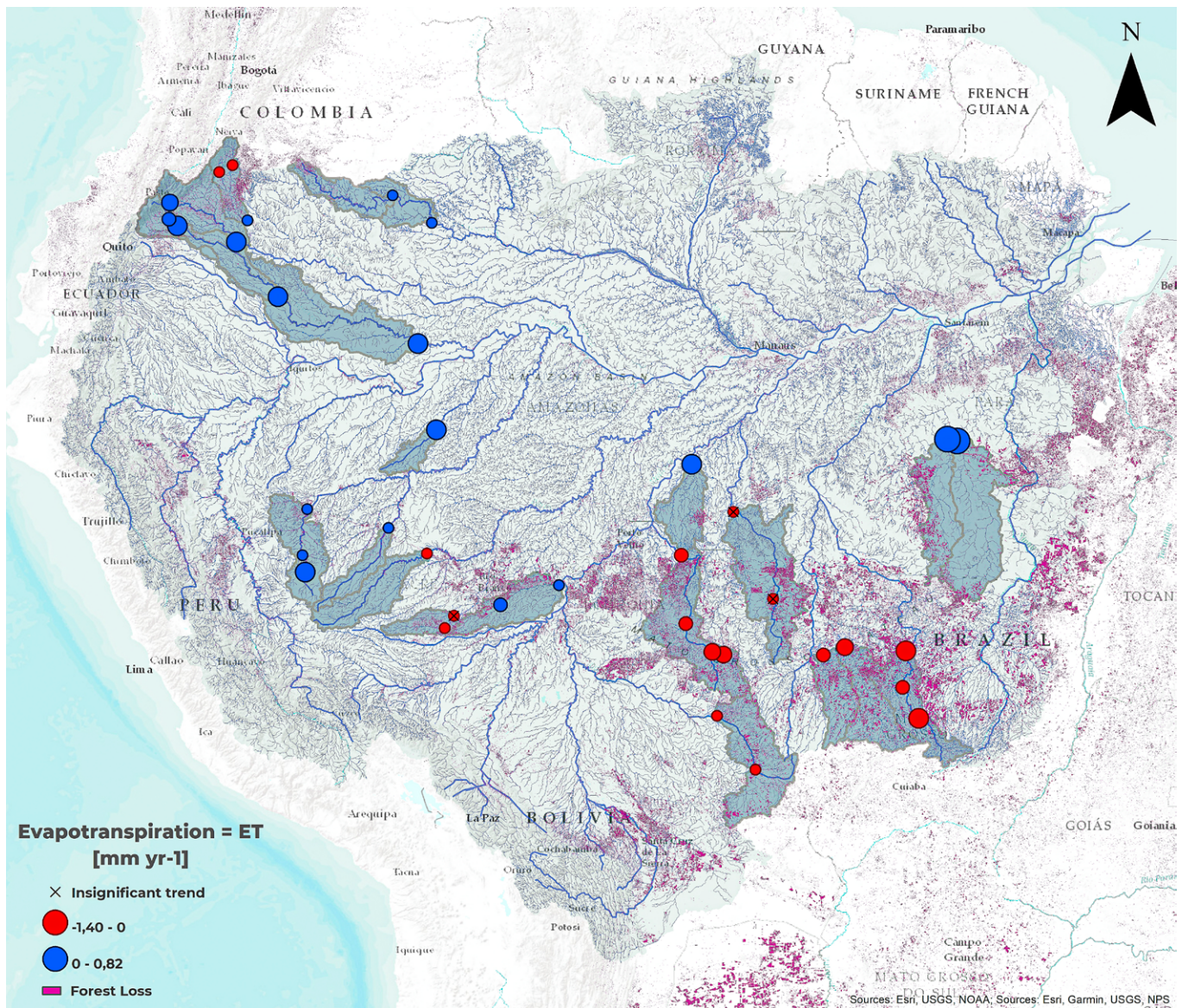
Figure 9. Similar to Fig. 7 for evapotranspiration trends in the selected sub-basins.

the day and in the opposite direction at night, which could explain why sun-basins with a higher percentage of deforestation show positive trends, while those that are deforested negative trends. Some studies have shown that changes in the variables of the hydrological cycle, especially in the rainfall regime, are more noticeable when the percentages of the deforested area are higher than 50% (Sampaio et al., 2007). In this work, the higher percentage of forest loss reaches 19.46%; however, we can see some evidence of the deforestation effect hydroclimatic trends. Aragão (2012) Explained that when rainfall over deforested areas is greater than rainfall over adjacent forests, it is because the increase in surface heat in deforested areas induces the upward movement of air, reducing pressure and dragging air from the areas with forests towards deforested areas, thus generating convective rain.

A predominant negative trend was found in time series of P, ET, and SM of sub-basins located in the "Arc of Deforestation," a region that experiences high anthropogenic change (Southeastern Amazon). Additionally, this region is characterized by dry seasonality, lower precipitation, where trees lose their leaves by the vegetation as a response to water stress (Da Rocha et al., 2009). A regional level Northern Amazonia was characterized for decreasing trends and positive trends in Southwestern Amazonia; these results are consistent with those found by Marengo (2004).

High precipitation in the Amazon depends upon the water vapor transported from the tropical Atlantic Ocean and evapotranspiration recycling from the forest. Hence, negative trends in precipitation may be associated with decreasing trends in evapotranspiration, associate with forest loss, particularly in the "Arc of Deforestation". At the same time, evapotranspiration is

Trend analysis of precipitation, evapotranspiration and soil moisture in regions under different regimes of forest loss in Amazonia

determined by the availability of water and energy on the earth's surface (Zhang et al., 2007). Suggested reasons for variations in actual evapotranspiration include changes in precipitation (Zhang et al., 2007), decrease in soil moisture content (Jung et al., 2010), non-opening of stomata due to high concentrations of CO_2 in the atmosphere, decreased in wind speed and changes in land use or land cover (Piao et al., 2007). More importantly, the increase of atmospheric demand (higher vapor pressure deficit) due to deforestation, especially in the Arc of Deforestation that experienced the big anthropogenic change (Barkhordarian et al., 2019), and radiation changes may explain the decrease in ET, taking into account that VPD and radiation as the most important mechanism that controls ET. In any event, the connection between evapotranspiration and precipitation is difficult to establish because it depends on a large number of interacting thermodynamic and dynamic processes, which must be taken into account quantitatively (Shukla & Mintz, 1982).

Higher rates of evapotranspiration can be observed during dry seasons due to the water stored after a wet season. However, in some regions, the precipitation is low and yet ET shows high values during dry season, something that can be explain for radiation, temperature and vapor pressure deficit variations (Guan et al., 2015)canopy photosynthesis of some tropical forests can decline, whereas in others it can be maintained at the same or a higher level than during the wet season. However, it remains uncertain to what extent water availability is responsible for productivity declines of tropical forests during the dry season. Here we use global satellite observations of two independent measures of vegetation photosynthetic properties (enhanced vegetation index from 2002 to 2012 and solar-induced chlorophyll fluorescence from 2007 to 2012.

CONCLUSIONS

The homogeneity of hydroclimatic times series in sub-basins of the Amazon River basin under different land covers were analyzed using four tests: the Pettit's test, the Buishand's test, and the Standard Normal Homogeneity test. This set of tests allowed us to detect a non-significant year of change in most of the analyzed series.

Decreasing evapotranspiration trends, soil moisture, and precipitation were found mainly over the "Arc of Deforestation" (southeastern Amazonia) and deforested areas of the Colombian Amazon. It is crucial to incorporate in the analysis how trends in water and energy contribute to changes in trend in evapotranspiration.

Results provide evidence of the hydrological impact of deforestation in the Amazon River basin, in particular about the drying out of the atmosphere over southern Amazonian as a result of human activities (Barkhordarian et al., 2019), in association with the identified decreasing trends in precipitation and soil moisture at sub-catchment scales.

Environmental information captured from satellites or generated from models constitutes an essential tool for research in environmental sciences and the study of the effects of global climate change. However, its application must be careful depending on the spatial resolution and the scale at which it is desired to work since otherwise, it can lead to inconsistencies in the results and even erroneous conclusions. For example, low-resolution raster information used in regional analyzes that require more detailed data and detailed analysis leads to errors, whereby detail is lost, and the contribution of the deforested area may not be seen.

REFERENCES

Abatzoglou, J. T., Dobrowski, S. Z., Parks, S. A., & Hegewisch, K. C. (2018). TerraClimate, a high-resolution global dataset of monthly climate and climatic water balance from 1958-2015. *Scientific Data*, *5*, 1-12. https://doi.org/10.1038/sdata.2017.191

Adarsh, S., & Shyma, M. (2017). Analyzing the non-linear trend and multiscale teleconnections of regional monsoon indices using empirical mode decomposition. *Modeling Earth Systems and Environment*, *3*(2), 669–682. https://doi.org/10.1007/s40808-017-0325-9

Ahmad, N. H., & Deni, S. M. (2013). Homogeneity Test on Daily Rainfall Series for Malaysia. *Matematika*, *29*(1), 141–150. http://www.matematika.utm.my/index.php/matematika/article/view/586

Alexandersson, H. (1986). A homogeneity test applied to precipitation data. *Journal of Climatology*, *6*(6), 661–675. https://doi.org/10.1002/joc.3370060607

Alexandersson, H., & Moberg, A. (1997). Homogemzation of Swedish temperature data. Part I: Homogeneity test for linear trends. *International Journal of Climatology*, *17*(1), 25–34. https://doi.org/10.1002/(sici)1097-0088(199701)17:1<25::aid-joc103>3.3.co;2-a

Almeida, C. T., Oliveira-Júnior, J. F., Delgado, R. C., Cubo, P., & Ramos, M. C. (2017). Spatiotemporal rainfall and temperature trends throughout the Brazilian Legal Amazon, 1973–2013. *International Journal of Climatology*, *37*(4), 2013–2026. https://doi.org/10.1002/joc.4831

Alves, L. M., Marengo, J. A., Fu, R., & Bombardi, R. J. (2017). Sensitivity of Amazon Regional Climate to Deforestation. *American Journal of Climate Change*, *06*(01), 75–98. https://doi.org/10.4236/ajcc.2017.61005

Aragão, L. E. O. C. (2012). The rainforest's water pump. *Nature*, *489*, 217–218.

Artaxo, P. Almeida-Val, P.V., Bilbao, B., Brando, P., Bustamante, M., Coe, M.T., Correa, S.B., Cuesta, F., Costa, M.H., Miralles–Wilhelm, F., Salinas, N., Silvério, D.V., and Val, A.L., (2021). Impacts of climate change on biodiversity, ecological processes, and environmental adaptation. Science Panel for the Amazon. Chapter 8. In the press.

Barkhordarian, A., Saatchi, S. S., Behrangi, A., Loikith, P. C., & Mechoso, C. R. (2019). A Recent Systematic Increase in Vapor Pressure Deficit over Tropical South America. *Scientific Reports*, *9*(1), 1–12. https://doi.org/10.1038/s41598-019-51857-8

Bonan, G. B. (2008). Forests and climate change: Forcings, feedbacks, and the climate benefits of forests. *Science*, *320*(5882), 1444–1449. https://doi.org/10.1126/science.1155121

Braun, S. A., Stocker, E., & Marius, J. (2011). *Tropical Rainfall Measuring Mission*. 1–58.

Buishand, T. A. (1984). "Test for Detecting a Shift in the Mean of Hydrological Time Series." *Journal of Hydrology*, *73*, 51–69.

Carmona, A. M., & Poveda, G. (2014). Detection of long-term trends in monthly hydro-climatic series of Colombia through Empirical Mode Decomposition. *Climatic Change*, *123*(2), 301–313. https://doi.org/10.1007/s10584-013-1046-3

Da Rocha, H. R., Manzi, A. O., Cabral, O. M., Miller, S. D., Goulden, M. L., Saleska, S. R., Coupe, N. R., Wofsy, S. C., Borma, L. S., Artaxo, R., Vourlitis, G., Nogueira, J. S., Cardoso, F. L., Nobre, A. D., Kruijt, B., Freitas, H. C., Von Randow, C., Aguiar, R. G., & Maia, J. F. (2009). Patterns of water and heat flux across a biome gradient from tropical forest to savanna in brazil. *Journal of Geophysical Research: Biogeosciences*, *114*(1), 1–8. https://doi.org/10.1029/2007JG000640

Foley, A., Fealy, R., & Sweeney, J. (2013). Model skill measures in probabilistic regional climate projections for Ireland. *Climate Research*, *56*(1), 33–49. https://doi.org/10.3354/cr01140

Guan, K., Pan, M., Li, H., Wolf, A., Wu, J., Medvigy, D., Caylor, K. K., Sheffield, J., Wood, E. F., Malhi, Y., Liang, M., Kimball, J. S., Saleska, S. R., Berry, J., Joiner, J., & Lyapustin, A. I. (2015). Photosynthetic seasonality of global tropical forests constrained by hydroclimate. *Nature Geoscience*, *8*(4), 284–289. https://doi.org/10.1038/ngeo2382

Hansen, M. C., Potapov, P. V., Moore, R., Hancher, M., Turubanova, S. A., Tyukavina, A., Thau, D., Stehman, S. V., Goetz, S. J., Loveland, T. R., Kommareddy, A., Egorov, A., Chini, L., Justice, C. O., & Townshend, J. R. G. (2013). High-resolution global maps of 21st-century forest cover change. *Science*, *342*(6160), 850–853. https://doi.org/10.1126/science.1244693

Huffman, G. J., Adler, R. F., Bolvin, D. T., Gu, G., Nelkin, E. J., Bowman, K. P., Hong, Y., Stocker, E. F., & Wolff, D. B. (2007). The TRMM Multisatellite Precipitation Analysis (TMPA): Quasi-global, multiyear, combined-sensor precipitation estimates at fine scales. *Journal of Hydrometeorology*, *8*(1), 38–55. https://doi.org/10.1175/JHM560.1

Jung, M., Reichstein, M., Ciais, P., Seneviratne, S. I., Sheffield, J., Goulden, M. L., Bonan, G., Cescatti, A., Chen, J., De Jeu, R., Dolman, A. J., Eugster, W., Gerten, D., Gianelle, D., Gobron, N., Heinke, J., Kimball, J., Law, B. E., Montagnani, L., … Zhang, K. (2010). Recent decline in the global land evapotranspiration trend due to limited moisture supply. *Nature*, *467*(7318), 951–954. https://doi.org/10.1038/nature09396

Kliment, Z., Matoušková, M., Ledvinka, O., & Královec, V. (2011). Trend analysis of rainfall-runoff regimes in selected headwater areas of the Czech Republic. *Journal of Hydrology and Hydromechanics*, *59*(1), 36–50. https://doi.org/10.2478/v10098-011-0003-y

Marengo, J. A. (2004). Interdecadal variability and trends of rainfall across the Amazon basin. *Theoretical and Applied Climatology*, *78*(1–3), 79–96. https://doi.org/10.1007/s00704-004-0045-8

Pettitt. (1979). A Non-parametric to the Approach Problem. *Applied Statistics*, *28*(2), 126–135.

Phillips, O. L., Malhi, Y., Higuchi, N., Laurance, W. F., Núñez, P. V., Vásquez, R. M., Laurance, S. G., Ferreira, L. V., Stern, M., Brown, S., & Grace, J. (1998). Changes in the carbon balance of tropical forests: Evidence from long- term plots. *Science*, *282*(5388), 439–442. https://doi.org/10.1126/science.282.5388.439

Piao, S., Friedlingstein, P., Ciais, P., De Noblet-Ducoudré, N., Labat, D., & Zaehle, S. (2007). Changes in climate and land use have a larger direct impact than rising CO2 on global river runoff trends. *Proceedings of the National Academy of Sciences of the United States of America*, *104*(39), 15242–15247. https://doi.org/10.1073/pnas.0707213104

Posada-Gil, D. and Poveda, G. (2015). Tendencias de largo plazo en los caudales de la cuenca amazónica y su relación con el área de la cuenca. Revista Colombia Amazónica, No. 8, Segunda Época, 123-136.

Poveda, G. (2020). Garantizar la integridad de los ecosistemas de Colombia: condición básica para preservar la biodiversidad y desarrollar la bioeconomía. En: C*iencia y tecnología: fundamento de la bioeconomía. Propuestas del Foco de Biotecnología, Bioeconomía y Medio Ambiente*. Volumen 3. Misión Internacional de Sabios. Vicepresidencia de la República de Colombia. Ministerio de Ciencia, Tecnología e Innovación. Universidad de los Andes, Bogotá, Colombia, pp. 55-97.

Rao, A. R., & Hsu, E.-C. (2008). Hilbert-Huang Transform Analysis Of Hydrological And Environmental Time Series. In *Hydrology and Water Resources of Africa* (Issue map C). https://doi.org/10.1007/0-306-48065-4

Sampaio, G., Nobre, C., Costa, M. H., Satyamurty, P., Soares-Filho, B. S., & Cardoso, M. (2007). Regional climate change over eastern Amazonia caused by pasture and soybean cropland expansion. *Geophysical Research Letters*, *34*(17). https://doi.org/10.1029/2007GL030612

Sayemuzzaman, M., & Jha, M. K. (2014). Seasonal and annual precipitation time series trend analysis in North Carolina, United States. *Atmospheric Research*, *137*, 183–194. https://doi.org/10.1016/j.atmosres.2013.10.012

Shukla, J., & Mintz, Y. (1982). Influence of land-surface evapotranspiration on the earth's climate. *Science*, *215*(4539), 1498–1501.

Zhang, X., Zwiers, F. W., Hegerl, G. C., Lambert, F. H., Gillett, N. P., Solomon, S., Stott, P. A., & Nozawa, T. (2007). Detection of human influence on twentieth-century precipitation trends. *Nature*, *448*(7152), 461–465. https://doi.org/10.1038/nature06025

Trend analysis of precipitation, evapotranspiration and soil moisture in regions under different regimes of forest loss in Amazonia

27